Supplementary Information for:

Ruthenium Nanoparticles Inside Porous $[Zn_4O(bdc)_3]$ by Hydrogenolysis of Adsorbed [Ru(cod)(cot)]: A Solid State Reference System for Surfactant Stabilized Ruthenium Colloids.

*Felicitas Schröder,[†] Daniel Esken,[†] Mirza Cokoja,[†] Maurits W. E. van den Berg,[#] Oleg I. Lebedev,[‡] Gustaaf Van Tendeloo, [‡] Bernadeta Walaszek,[§] Gerd Buntkowsky,[§] Hans-Heinrich-Limbach,[+] Bruno Chaudret[‖] and Roland A. Fischer[†],**

[†]Anorganische Chemie II - Organometallics & Materials, Ruhr-Universität Bochum, Universitätsstrasse 150, D-44780 (Germany). † Anorganische Chemie II - Organometallics & Materials, Ruhr-Universität, D-44870 Bochum, Germany. #Technische Chemie, Ruhr-Universität, D-44870 Bochum, Germany. ‡EMAT, University of Antwerp, Groenenborgerlaan 171, B-2020 Antwerp, Belgium.§Institut für Physikalische Chemie, Friedrich-Schiller-Universität, D-07743 Jena Jena, Germany.+Physikalische und Theoretische Chemie, Freie Universität, D-11195 Berlin, Germany. ‖Laboratoire de Chimie de Coordination-CNRS, F-31077 Toulouse Cedex 4, France.

FT-IR spectrum of [Ru(cod)(cot)]@MOF-5

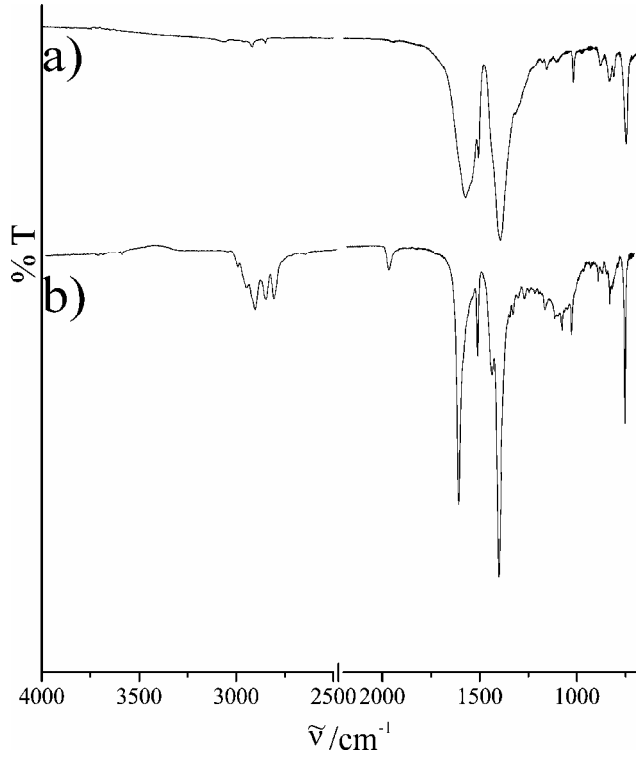

Figure 1S. FT-IR spectra of empty MOF-5 (a) and $[Ru(cod)(cot)]_{3.5}$@MOF-5 (**2**) (b) additional vibrational bands in (b) are derived from precursor inclusion.

^{13}C-MAS-NMR of Ru(cod)(cot)

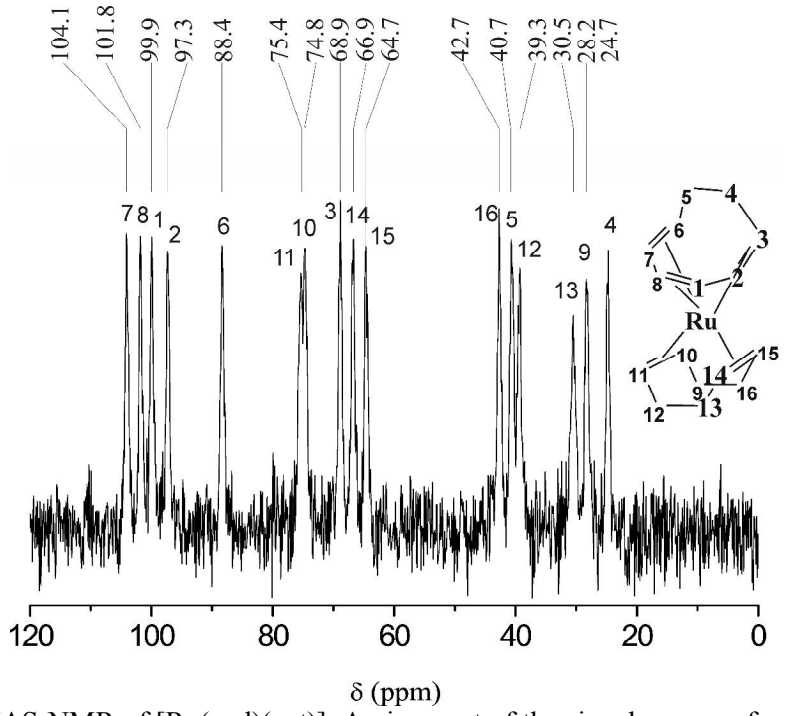

Figure 2S. ^{13}C-MAS-NMR of [Ru(cod)(cot)]. Assignment of the signals was performed by simulation of the spectrum with Gaussian 03 (B3LYP/GIAO; Ru: Stuttgart RSC 1997; C,H: 6-31 G*)

Thermal isomerization of [Ru(cod)(cot)] in MOF-5: ^{13}C-MAS-NMR

After loading MOF-5 at 60°C in 10^{-5} mbar for 6 days, a mixture of [Ru(cod)(cot)] and bis(η^5-cyclooctadienyl)ruthenium in MOF-5 was obtained as detected by ^{13}C-MAS-NMR.

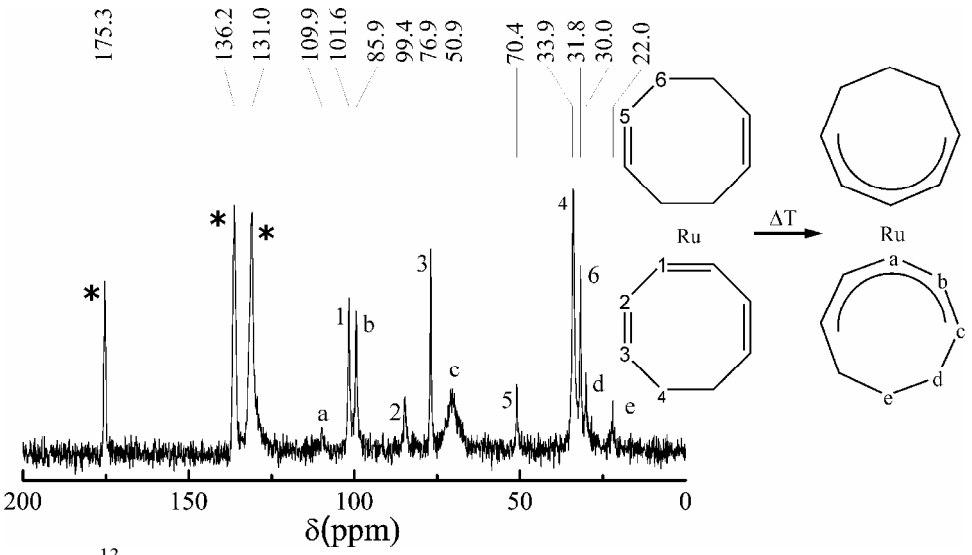

Figure 3S. ^{13}C-MAS-NMR of a mixture of [Ru(cot)(cot)] and bis(η^5-cyclooctadienyl)ruthenium in MOF-5.

Hydrogenolysis of [Ru(cod)(cot)]$_{3.5}$@MOF-5 (2) at mild conditions: XAS and TEM results

In order to investigate the oxidation state and chemical environment of the hydrogenation product of [Ru(cod)(cot)]@MOF-5 at mild conditions, XAS measurements of the resulting material {[Ru(cod)]/Ru}@MOF-5 (**2**) were performed. The XANES and EXAFS of the material correspond to the XANES and EXAFS for Ru@MOF-5 (Fig. 4S) indicating that most of the Ru precursor is converted to Ru in the metallic state already after short hydrogenation.

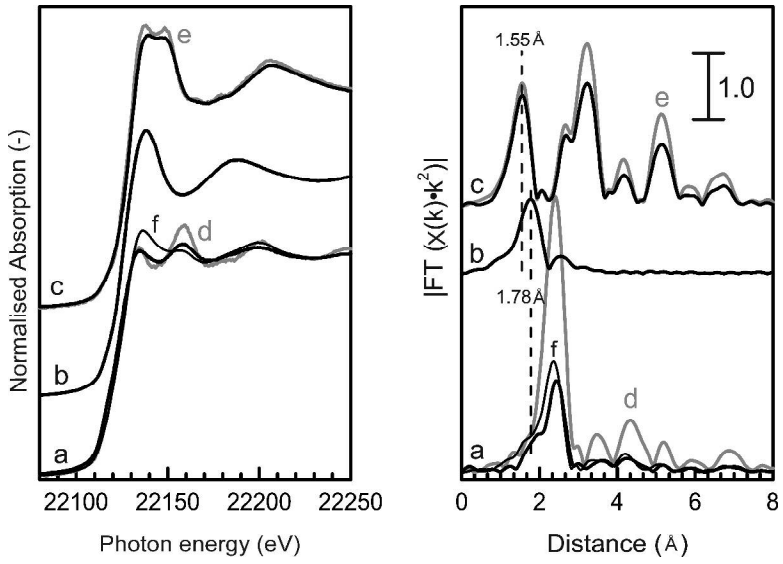

Figure 4S. XANES (left) and EXAFS (right) of (a) Ru@MOF-5 (**4**), (b) [Ru(cod)(cot)]3.5@MOF-5 (**2**), (c) Ru-ox@MOF-5 and (f) {[Ru(cod)]/Ru}@MOF-5 (**3**) compared to (d) Ru foil and (e) RuO_2. All data were recorded at liquid nitrogen temperature, except the Ru foil, which was recorded at room temperature.

A representative TEM picture of the material is given in Figure 5S. It clearly depicts the characteristic pore architecture of the MOF host material. It also shows the incorporation of Ru metal nanoparticles inside the host material and a uniform distribution of the particles throughout the framework, confirmed by EDX analysis.

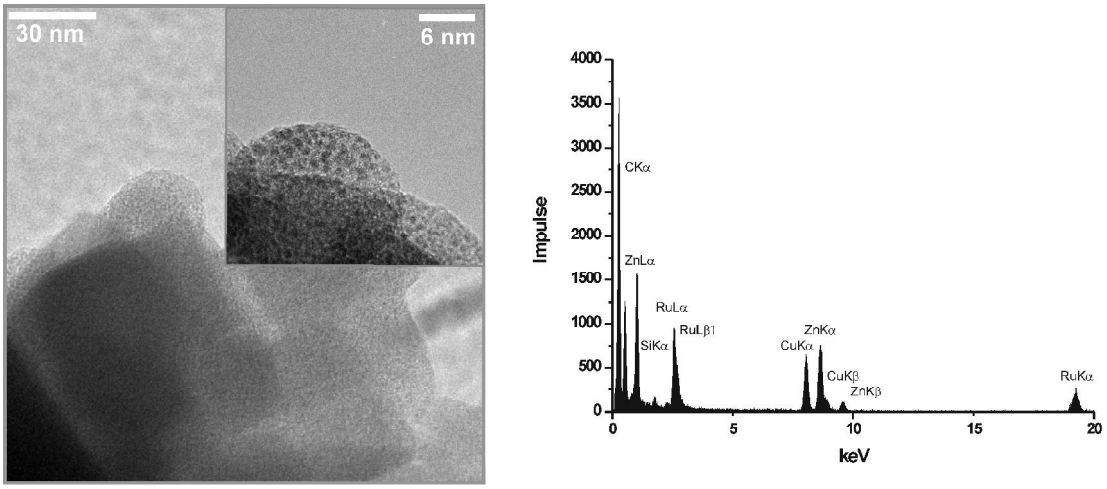

Figure 5S. TEM picture and EDX spectrum of [Ru(cod)(cot)]@MOF-5 after hydrogenation in 1 sccm H_2, 25°C, 30 min.

The Ru nanoparticles can be observed as regions of higher contrast due to the higher number of electrons in the metal compared to the metal oxide bases host material. The particles are in a size range of 1.6-1.8 nm. From N_2-sorption measurements of the material a reduced Langmuir surface area of 1600 m^2/g was calculated, this is a decrease of nearly 50% in comparison to the "empty" MOF-5 powder which had a specific surface area of 3300 m^2/g prior to the loading with precursor and subsequent hydrogenation. Again, the decrease of the surface area is due to the formation of Ru nanoparticles inside the framework.

Quantitative hydrogenation of [Ru(cod)(cot)]@MOF-5 to yield Ru@MOF-5 (4): ^{13}C-MAS-NMR

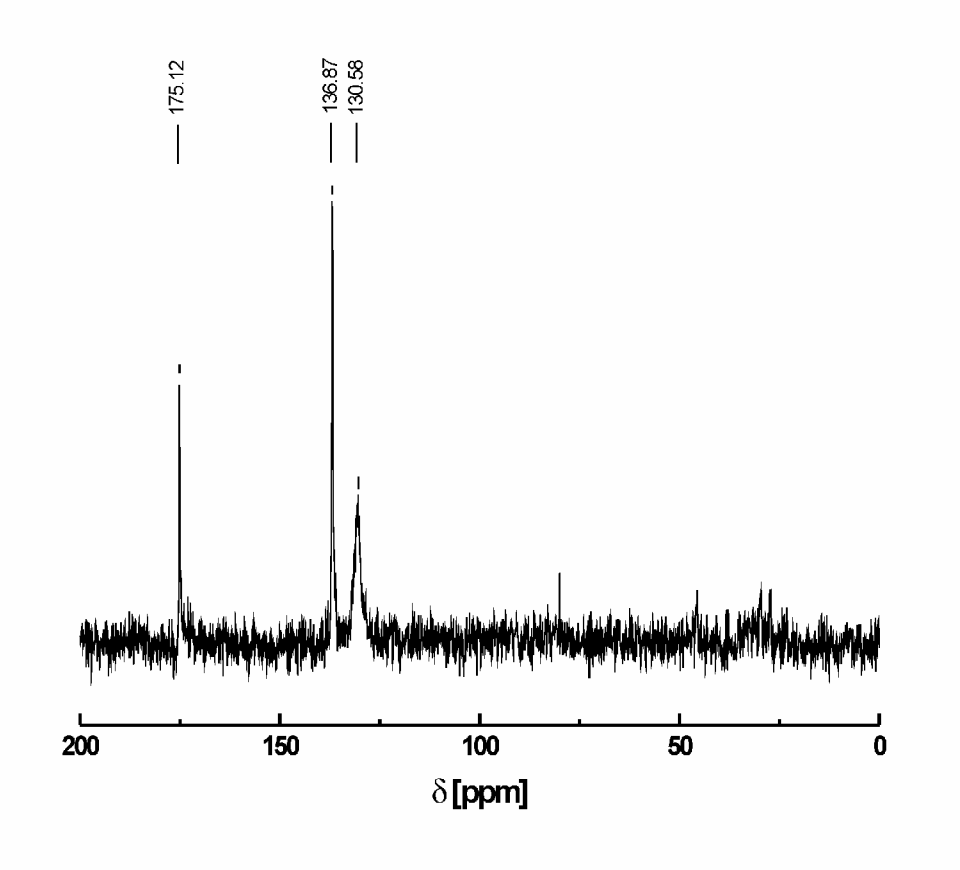

Figure 6S. ^{13}C-MAS-NMR of Ru@MOF-5 (**4**), only signals from the intact MOF-5 framework are observed.

PXRD of Ru@MOF-5 (4)

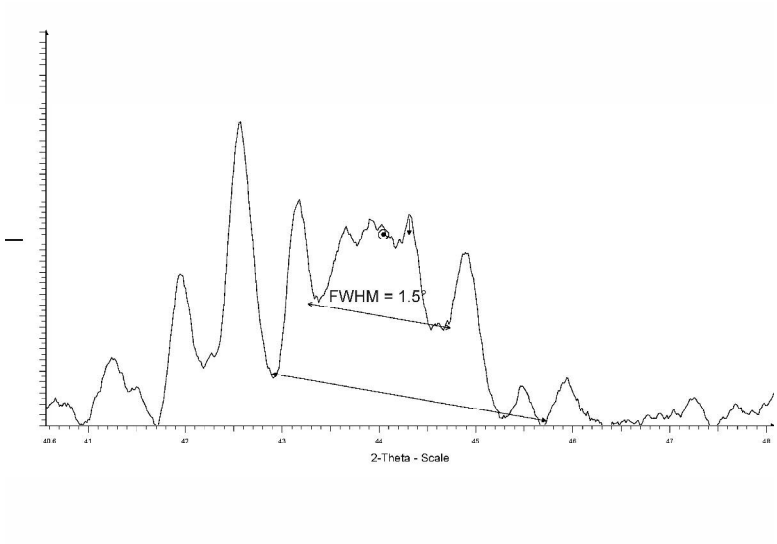

Figure 7S. Estimation of the FWHM (full width at half maximum) of the Ru (101) reflection in the powder XRD diffractogramm of Ru@MOF-5 (**4**). Screenshot of Bruker Diffrac Plus Eva 2004 software, version 10.0. The determination of the FWHM is certainly difficult because of the superposition of the MOF reflections and the low intensity of the peak. Certainly, a sharper peak could be hidden under the many other reflections. Look at the Figure 11S below, which shows the material after calcination at 500 °C and total break-down of the matrix.

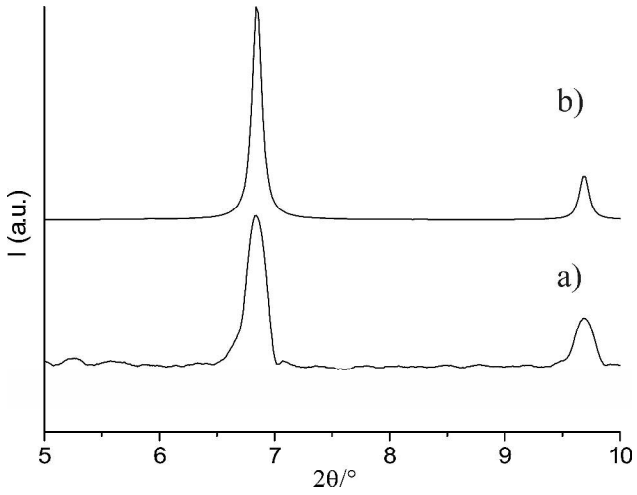

Figure 8S. Low angle powder XRD diffractogramms of (a) Ru@MOF-5 (**4**) and (b) pure, activated MOF-5.

In the pure, activated MOF-5 the relative intensity ratio of the reflections at 6.9° and 9.7° was found to be 1 : 0.51. As discussed above, in the low angle XRD of $[Ru(cod)(cot)]_{3.5}$@MOF-5 (**2**) the intensities of these two peaks are inverted with an intensity ratio of 0.25 (6.9 °) : 1 (9.7°). For Ru@MOF-5 (**4**) (see Figure 8Sa), the peaks at 6.9° and 9.7 ° exhibit an intensity ratio of 1 : 0.75. Here, the intensity decrease of the reflection at 6.9° is not as pronounced as in $[Ru(cod)(cot)]_{3.5}$@MOF-5 (**2**) but a difference in intensity compared to the low angle PXRD of pure MOF-5 (Figure 8Sb) is clearly detected.

TEM measurements of Ru@MOF-5 (4):

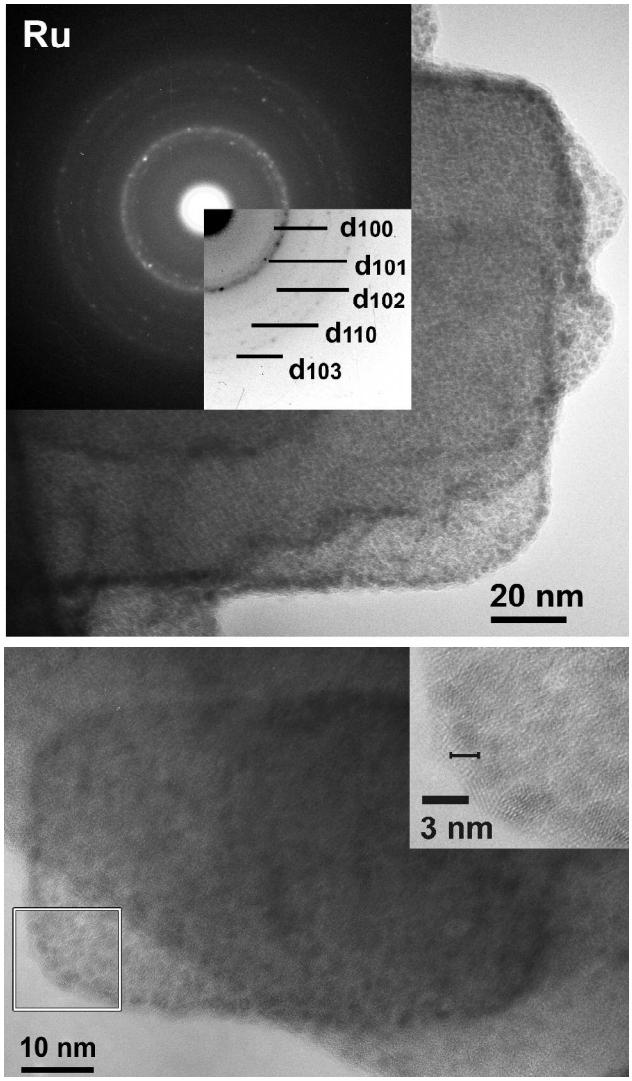

Figure 9S(a). TEM pictures of Ru@MOF-5 (**4**). The pictures presented here exhibit a lower resolution than the ones shown in the main text. The corresponding sample was prepared on a standard Cu grid (300 mesh, with carbon film). For the pictures shown in the main text and the tomographical measurements, Cu grids (300 mesh, with holey carbon film) were used in order to obtain a higher resolution.

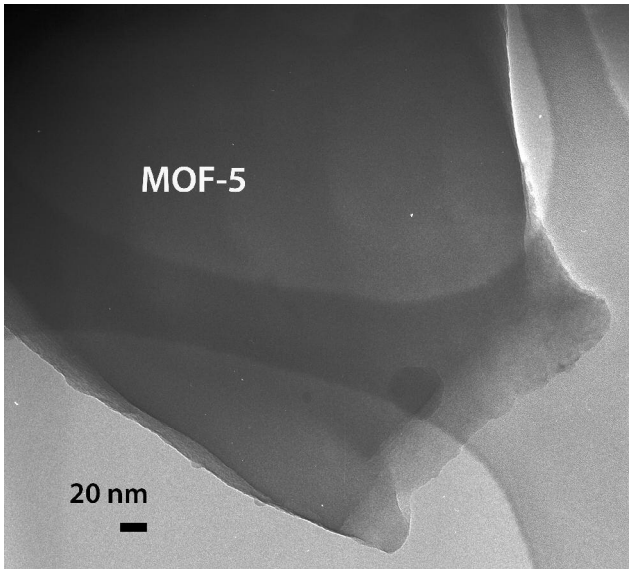

Figure 9S(b). TEM picture of pure MOF-5.

Tomographical TEM measurements of Ru@MOF-5 (4)

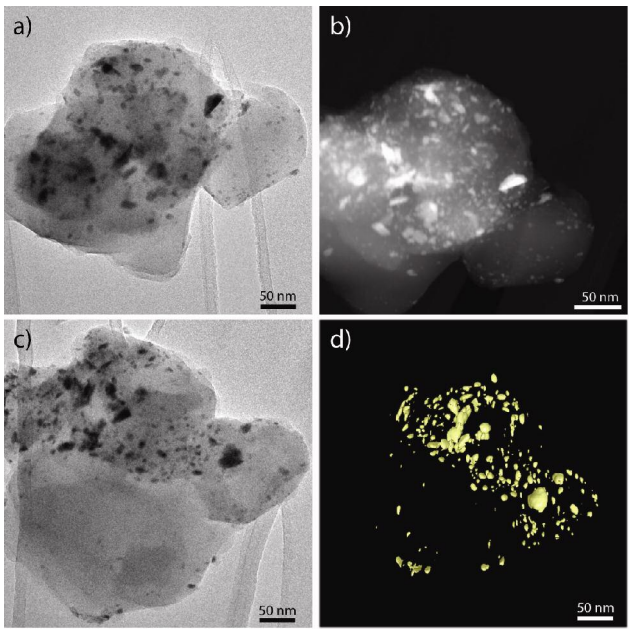

Figure 10S. (a) Bright field TEM image taken at 0º tilt. It can be seen that the MOF 5 material is made up of faceted crystals. (b) HAADF image taken in the same orientation as a). The Ru-particles (white contrast) can be clearly distinguished. (c) Bright field TEM image taken at tilt angle of -60º. Tomographically reconstructed 3D image of the Ru-particles within the four MOF crystals. The orientation is approximately as in c).

Figure 10Sa presents a TEM picture of four MOF-5 nanocrystallites from sample **4**. The three top crystals have a high Ru-particle (black contrast) density, in the bottom crystal only few Ru-particles are imbedded. Obviously larger regions of higher contrast can be seen in the pictures. Note that the TEM pictures presented in Fig. 10S were taken at medium magnification, therefore a distinction between large particles and agglomerations of smaller individual particles is not possible. For better resolved TEM pictures see main text, Figure 7. Upon higher magnification, the displayed regions of higher contrast in Figure 10S(a) appear as images that are similar to the ones shown in the main text. Since we did not detect sharp powder XRD reflections for Ru in the sample presented in Figure 10S, we believe that the regions of higher contrast with a diameter above 3 nm are agglomerates of smaller actually separated particles. Nevertheless, Figure 10S clearly shows that the Ru nanoparticles are distributed throughout the MOF-5 crystallites and are not exclusively located at the surface of the crystallites. In addition note that TEM sample preparation breaks down the individual microcrystals into pieces. We are not looking at "single nanocrystallites", but to pieces of larger crystalls.

Temperature Stability of Ru@MOF-5

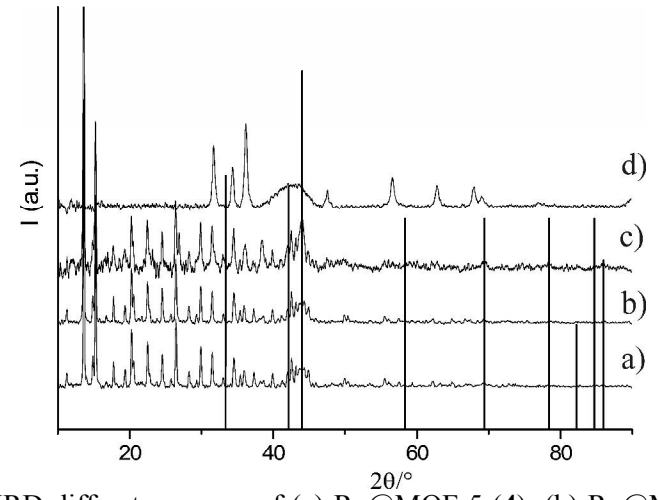

Figure 11S. Powder XRD diffractogramms of (a) Ru@MOF-5 (**4**); (b) Ru@MOF-5 after calcination at 200°C; 14 h, (c) Ru@MOF-5 after calcination at 400°C, 14 h; (d) Ru@MOF-5 after calcination at 500°C, 14 h.

As discussed in the main text, only a very broad reflection for Ru (101) can be observed in the XRD of Ru@MOF-5 (**4**). In order to further investigate the embedding of the Ru nanoparticles in MOF-5, calcination studies in vacuo (10^{-3} mbar) were performed at 200°C, 400°C and 500°C. Calcination at 500°C leads to complete decomposition of MOF-5 to ZnO, assigned by the reflections at 31.8°, 34.4°, 36.3°, 47.5°, 56.6°, 62.9°, 67.9° and 69.10°. However, even after calcination at 500°C alomost no sharpening of the Ru reflection at 44.006° 2θ is observed compared to the original broad reflection shown in Figure 11S(a). In contrast to that, particles located outside the framework should exhibit sharper reflections after calcination at elevated temperatures due to agglomeration processes. However no sharp superpositions of the peak are seen. The calcination experiments therefore additionally confirm the embedding of the Ru nanoparticles in MOF-5 – and even the stabilisation after calcination and matrix break-down (possibly by the ZnO formed, as known from typical supported catalysts).

Oxidation of Ru@MOF-5 (4)

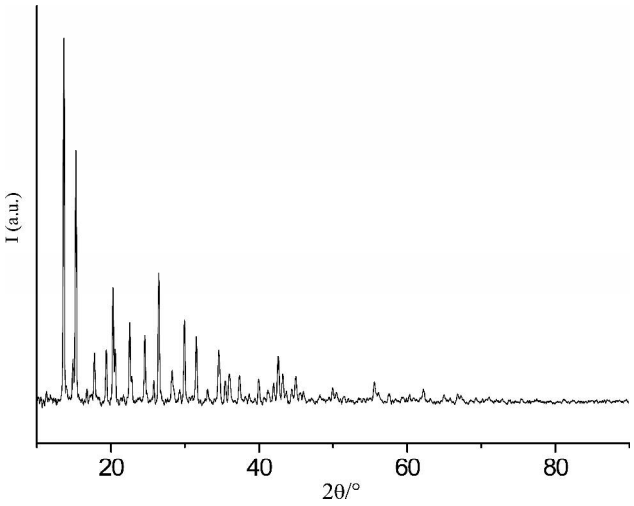

Figure 12S. Powder XRD diffractogramm of Ru@MOF-5 (**4**) after oxidation.

Hydrogenation of benzene by Ru@MOF-5

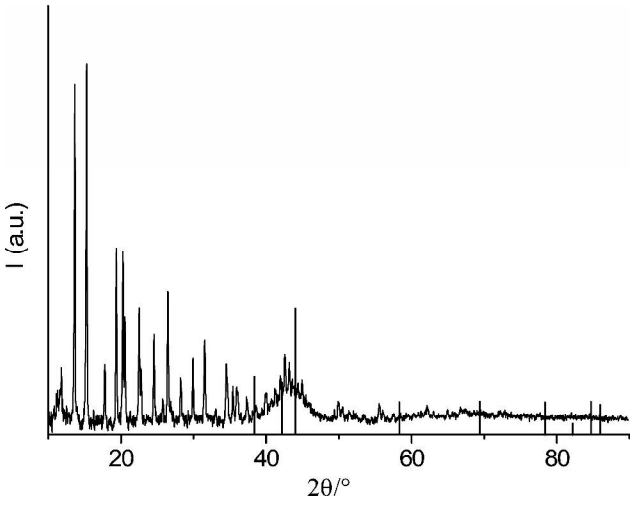

Figure 13S. Powder XRD diffractogramm of Ru@MOF-5 after the catalytical hydrogenation of benzene. (Lines: Ru JPDS reference No. 6-0663).

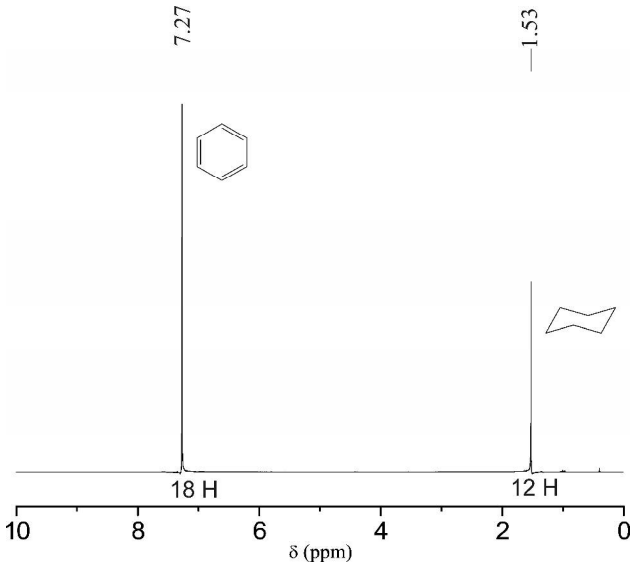

Figure 14S. ^{1}H-NMR spectrum (in C_6D_6) of the filtrate from the hydrogenation catalysis. The corresponding integrals are assigned in numbers of H-Atoms.